

Search for Standard Model Higgs Boson in $H \rightarrow WW$ Channel at CDF

J. Pursley, on behalf of the CDF Collaboration

Department of Physics, University of Wisconsin-Madison, Madison, WI, 53706, USA

We present a search for standard model (SM) Higgs boson to $WW^{(*)}$ production in dilepton plus missing transverse energy final states in data collected by the CDF II detector corresponding to 4.8 fb^{-1} of integrated luminosity. To maximize sensitivity, the multivariate discriminants used to separate signal from background in the opposite-sign dilepton event sample are independently optimized for final states with zero, one, or two or more identified jets. All significant Higgs boson production modes (gluon fusion, associated production with either a W or Z boson, and vector boson fusion) are considered in determining potential signal contributions. We also incorporate a separate analysis of the same-sign dilepton event sample which potentially contains additional signal events originating from associated Higgs boson production mechanisms. Cross section limits relative to the combined SM predictions are presented for a range of Higgs boson mass hypotheses between 110 and 200 GeV/c^2 .

1. Introduction

The Higgs boson is introduced into the SM to explain electroweak symmetry breaking and the origins of particle mass. This paper presents an analysis searching for a Higgs boson decaying to $WW^{(*)}$, which is the dominant decay mode for $m_H > 135 \text{ GeV}/c^2$ [1]. The small cross section of the dominant gluon fusion production mechanism ($\sigma_{NNLL}(gg \rightarrow H) = 0.439 \text{ pb}$ for $m_H = 160 \text{ GeV}/c^2$ [2, 3, 4]) makes observation of the signal difficult within the hadron collider environment. This analysis searches for $H \rightarrow WW^{(*)} \rightarrow \ell^+ \ell^- \nu \bar{\nu}$, where $\ell = e, \mu, \text{ or } \tau$ with final states $e^+ e^-$, $e^\pm \mu^\mp$, and $\mu^+ \mu^-$. In addition, a search is made for associated Higgs boson production in events with two like-sign dileptons, with final states $e^\pm e^\pm$, $e^\pm \mu^\pm$, and $\mu^\pm \mu^\pm$. The data corresponds to 4.8 fb^{-1} of integrated luminosity collected at the Fermilab Tevatron in $p\bar{p}$ collisions at $\sqrt{s} = 1.96 \text{ TeV}$.

2. Event Selection

The CDF II detector is described in detail in Ref. [5]. The geometry of the detector is characterized by the azimuthal angle ϕ and the pseudorapidity $\eta = -\ln[\tan(\theta/2)]$, where θ is the polar angle measured from the proton beam direction. The transverse energy $E_T = E \sin \theta$, where E is the energy in the calorimeter towers associated with a cluster of energy deposition. Transverse momentum p_T is the track momentum component transverse to the beam-line. The missing transverse energy vector \vec{E}_T is defined as $-\sum_i E_T^i \hat{n}_T^i$, where \hat{n}_T^i is the transverse component of the unit vector pointing from the interaction point to the energy deposition in calorimeter tower i . This is corrected for the p_T of muons, which do not deposit all of their energy in the calorimeter, and tracks which point to uninstrumented regions in the calorimeter. The missing transverse energy \cancel{E}_T is defined as $|\vec{E}_T|$. Strongly interacting partons produced

in the $p\bar{p}$ collision undergo fragmentation that results in highly collimated jets of hadronic particles. Jet candidates are reconstructed using the calorimeter towers with corrections to improve the estimated energy [6] and are required to have $E_T > 15 \text{ GeV}$ and $|\eta| < 2.5$.

The $\ell\ell\nu\bar{\nu}$ candidates are selected from two opposite-sign (OS) leptons. At least one lepton is required to satisfy the real-time trigger selection and have $p_T > 20 \text{ GeV}/c$. This requirement is loosened to $10 \text{ GeV}/c$ for the second lepton to increase Higgs boson kinematic acceptance. The z -positions of the leptons in a candidate at the point of closest approach to the beam-line are required to be within 4 cm of each other to reduce backgrounds from overlapping $p\bar{p}$ collisions.

There are several sources of background with the same or a similar final state: $WW \rightarrow \ell\ell\nu\bar{\nu}$, $ZZ \rightarrow \ell\ell\nu\bar{\nu}$ or $\ell\ell\ell\ell$, $WZ \rightarrow \ell\ell\nu$ or $\ell\nu\nu\bar{\nu}$, $t\bar{t} \rightarrow b\bar{b}\ell\ell\nu\bar{\nu}$, Drell-Yan (DY) $Z \rightarrow \ell\ell$ where the measured large \cancel{E}_T is due to resolution tails, $W\gamma$ where the photon converts to an e^-e^+ pair, and W +jets where a jet is misidentified as a lepton. To reduce the contribution of $W\gamma$ and W +jets, all leptons must be isolated with requirements on both the surrounding E_T in the calorimeters and p_T of surrounding tracks. Candidates are further required to have a dilepton invariant mass $M_{\ell\ell} > 16 \text{ GeV}/c^2$ to suppress $W\gamma$, and exactly 2 leptons to suppress contributions with additional leptons.

To reduce the DY background, we require $\cancel{E}_{T\text{spec}} > 25 \text{ GeV}$ (reduced to $\cancel{E}_{T\text{spec}} > 15 \text{ GeV}$ for electron-muon events where DY background is inherently smaller), where

$$\cancel{E}_{T\text{spec}} \equiv \begin{cases} \cancel{E}_T & \text{if } \Delta\phi_{\cancel{E}_T, \text{nearest}} > \frac{\pi}{2} \\ \cancel{E}_T \sin(\Delta\phi_{\cancel{E}_T, \text{nearest}}) & \text{if } \Delta\phi_{\cancel{E}_T, \text{nearest}} < \frac{\pi}{2} \end{cases}$$

The $\Delta\phi_{\cancel{E}_T, \text{nearest}}$ is the azimuthal separation between the \vec{E}_T and the momentum vector of the nearest lepton or jet candidate. With this definition, we require the missing energy transverse to the nearest lepton or jet in the event to be greater than the minimum threshold if \vec{E}_T points along that object. Thus a mis-

measurement of the energy of one lepton or jet candidate would not allow the event to enter the sample.

We consider individually final states with zero, one, or two or more jet candidates in the event. This allows us to tune our multivariate discriminants on the different relative sizes of signal and background contributions within each jet multiplicity bin. The dominant background in the zero jet bin is WW , while in the one jet bin the background from DY is of a similar size as the WW background. The dominant background in the two or more jets bin is $t\bar{t}$ production. To suppress the $t\bar{t}$ contribution, all events with two or more jets containing one or more jets with a tight, secondary vertex b -tag are rejected. After all selection requirements we observe (summing over all jet multiplicities) a total of 1467 candidate events compared against an expectation of 1479 ± 141 background events and 25 ± 3 signal events for a SM Higgs boson with a mass of $165 \text{ GeV}/c^2$.

2.1. Event Selection for Same Sign Analysis

Like-sign, or same-sign (SS), dileptons occur in $VH \rightarrow VWW$ production when the vector boson (Z or W) and one of the W bosons from the Higgs boson decays leptonically. The dominant backgrounds to this search are from the charge mismeasurement of a real lepton, photon conversion to e^-e^+ , and misidentification of a jet as a lepton.

The event selection for OS events is modified to select two like-sign leptons and reduce potential backgrounds. The SS channel does not use forward electron candidates, which have a high rate of charge mismeasurement. To reduce the numbers of conversion electrons and jets misidentified as leptons, the p_T requirement for the second lepton is increased from 10 to 20 GeV/c . As the decay of the third boson most often results in the production of additional jets, we also require one or more jet candidates in the final state. Like-sign VH events tend to have lower values of \cancel{E}_T because the neutrinos are not necessarily back-to-back. To increase the signal acceptance, no $\cancel{E}_{T\text{spec}}$ requirement is made. After all selection requirements we observe a total of 64 candidate events compared against an expectation of 62 ± 11 background events and 1.7 ± 0.2 signal events for a SM Higgs boson with a mass of $165 \text{ GeV}/c^2$.

3. Data Modeling

The geometric and kinematic acceptance for the WW , WZ , ZZ , $W\gamma$, DY , $t\bar{t}$, and all of the signal processes ($gg \rightarrow H$, WH , ZH , VBF) are determined using a Monte Carlo calculation of the collision followed by a GEANT3-based simulation of the CDF II

detector response [7]. The Monte Carlo generator used for WW is MC@NLO [8], while for WZ , ZZ , DY , $t\bar{t}$, and the signal processes PYTHIA [9] is used, and $W\gamma$ is modeled with the generator described in Ref. [10]. We use the CTEQ5L [11] parton distribution functions (PDF) to model the momentum distribution of the initial-state partons.

The expected yields of background processes are normalized to cross sections calculated at partial next-to next-to-leading order ($t\bar{t}$ [12]), next-to-leading order (WW , WZ , and ZZ [13]), or leading-order with estimated higher-order corrections ($W\gamma$ [10] and DY [14]). The gluon fusion cross section has been calculated to next-to next-to-leading logarithmic accuracy [2, 3, 4]. Associated production cross sections at next-to next-to-leading order (NNLO) are obtained from Ref. [15]. VBF cross sections at next-to-leading order (NLO) are obtained from Ref. [16].

The background from W +jets is estimated from a sample of data events with one identified lepton and one jet that fulfills loose isolation requirements and contains a track or energy cluster similar to those required for lepton identification. The contribution of each event to the total yield is scaled by the probability that such a jet is identified as a lepton. This probability is determined from multijet events collected in independent jet-triggered data samples. A correction is applied for the small real lepton contribution using single W and Z boson Monte Carlo simulation.

4. Cross Checks

Several control regions are constructed to validate different aspects of the data modeling. The sample sizes of the control regions are designed to be large enough to give statistically meaningful tests. These control regions, described below, show good agreement between the background model predictions and the observed distributions in data.

One of the most fundamental control regions is the Drell-Yan sample selected using the default OS candidate selection in Sec. 2 with a reversed $\cancel{E}_T < 25 \text{ GeV}$ (15 GeV in the case of $e\mu$ events) requirement and the additional requirement that the dilepton invariant mass fall in the Z mass region. This control sample provides a high statistics test of acceptance, lepton identification efficiency, and trigger efficiency calculations.

A W +jets control sample is constructed from events which satisfy the SS candidate selection in Sec. 2.1 but have zero jet candidates. This control sample contains contributions primarily from jets misidentified as leptons, with additional contributions from conversion electrons and charge mismeasurement of a real lepton, and checks the modeling of misidentified particles.

A $t\bar{t}$ control sample is constructed using the default OS candidate selection in Sec. 2 with a requirement

of two or more jets in the event, and the b -tag veto requirement reversed such that only events with one or more jets with a b -tag are accepted.

A second DY control sample tests the \cancel{E}_T model, and is constructed using the default OS candidate selection in Sec. 2 with the exception of requiring $15 < \cancel{E}_{T\text{spec}} < 25$ GeV instead of $\cancel{E}_{T\text{spec}} > 25$ GeV (in the case of $e\mu$ events, $10 < \cancel{E}_{T\text{spec}} < 15$ GeV instead of $\cancel{E}_{T\text{spec}} > 15$ GeV). No requirements are made on the jet multiplicity or the dilepton invariant mass.

5. Analysis Technique

For each search channel, a NeuroBayes[®] [17] neural network is trained on a weighted combination of signal and background events from Monte Carlo independently for each Higgs boson mass hypothesis (14 total). Each neural network has three layers consisting of input nodes, hidden nodes, and one output node. Once the neural network is trained, templates are created for all signal and background processes. For the OS zero and one jet channels, “high S/B” and “low S/B” templates based on the signal-to-background ratio of the different dilepton combinations are considered separately. The templates are used as the final discriminant in calculating the 95% credibility level (C.L.) limits.

The OS zero jet channel uses 5 input variables. The inputs are: the ΔR between the leptons, the $\Delta\phi$ between the leptons, the scalar sum of the leptons’ p_T and the \cancel{E}_T , the likelihood ratio for Higgs to WW production (LR_{HWW}), and the likelihood ratio for WW production (LR_{WW}). The likelihood ratios are determined using a matrix element method which calculates the probability for each event to have been produced by several relevant SM processes.

The OS one jet channel uses 8 input variables. The inputs are: the $M_{\ell\ell}$, the transverse mass of the sum of the leptons’ 4-momenta and $(\cancel{E}_T, \text{MetX}, \text{MetY}, 0)$ where MetX and MetY are the x and y components of the $\vec{\cancel{E}}_T$, the ΔR between the leptons, the scalar sum of the leptons’ p_T and jets’ E_T and the \cancel{E}_T (H_T), the $\cancel{E}_{T\text{spec}}$, the leading lepton p_T , the subleading lepton p_T , and the leading lepton energy.

The OS two or more jets channel uses 8 input variables. The inputs are: the $M_{\ell\ell}$, the leading lepton p_T , the subleading lepton p_T , the H_T , the ΔR between the leptons, the $\Delta\phi$ between the leptons, the $\Delta\phi$ between the vector sum of the leptons’ p_T and the $\vec{\cancel{E}}_T$, and the vector sum of the first and second jet E_T .

The SS one or more jets channel uses 13 input variables. The inputs are: the $M_{\ell\ell}$, the leading lepton energy, the leading lepton p_T , the subleading lepton p_T , the H_T , the leading jet E_T , the $\Delta\phi$ between the leptons, the vector sum of all jets’ E_T , the vector sum of

leptons’ p_T , the \cancel{E}_T , the \cancel{E}_T significance ($\cancel{E}_T/\sqrt{\Sigma E_T}$), the $\cancel{E}_{T\text{spec}}$, and the $\Delta\phi_{\cancel{E}_T, \text{nearest}}$.

Neural network outputs are shown in Figure 1 for each channel at a Higgs boson mass of 165 GeV/ c^2 . Plots of the input variables and neural network outputs for all Higgs boson masses are available in Ref. [18].

6. Systematics

Systematic uncertainties associated with the Monte Carlo simulation affect the signal, WW , WZ , ZZ , $W\gamma$, DY, and $t\bar{t}$ acceptances taken from the simulated event samples. Uncertainties originating from lepton selection and trigger efficiency measurements are propagated through the acceptance calculation, giving uncertainties typically around 2%, but as high as 7% for the different signal and background processes. For the SS channel, there is an additional systematic for the simulated backgrounds which enter the sample only when a lepton’s charge is mismeasured (WW , $t\bar{t}$, and DY) which is taken as half the difference between the mismeasurement rates found in DY events and those found in Monte Carlo.

We also assign an acceptance uncertainty due to potential contributions from higher-order effects. In the case of WW we take half of the difference between the leading-order (PYTHIA-based [9]) and next-to-leading order (MC@NLO [8]) acceptances. The other processes are only simulated at leading-order and for these modes we assign the full difference observed in WW , leading to a 10% uncertainty. The largest uncertainty on the Drell-Yan process originates from modeling of the fake \cancel{E}_T in these events. Based on discrepancies in the DY \cancel{E}_T control region, we assign a 20% uncertainty in the zero jet channel and 25% uncertainties in the one and two or more jets channels. For processes that produce no final state jets at leading-order (WW , $W\gamma$, and DY), we also assign a jet modeling systematic to account for uncertainties in the Monte Carlo modeling of the p_T boost and additional jet production from initial and final state radiation. The uncertainties for these effects are anti-correlated between jet channels since the effect of extra jet production is to move events from one channel to another. For Monte Carlo samples not currently generated over the entire data run range, we take additional uncertainties on the acceptance for the corresponding signal or background process. This uncertainty comes from the observed difference in the leading-order WW acceptance for the corresponding partial run range versus that for the full run range. The acceptance variations due to PDF model uncertainties is assessed to be on the order of 2% using the 20 pairs of PDF sets described in Ref. [19].

For the $W\gamma$ background contribution, there is an

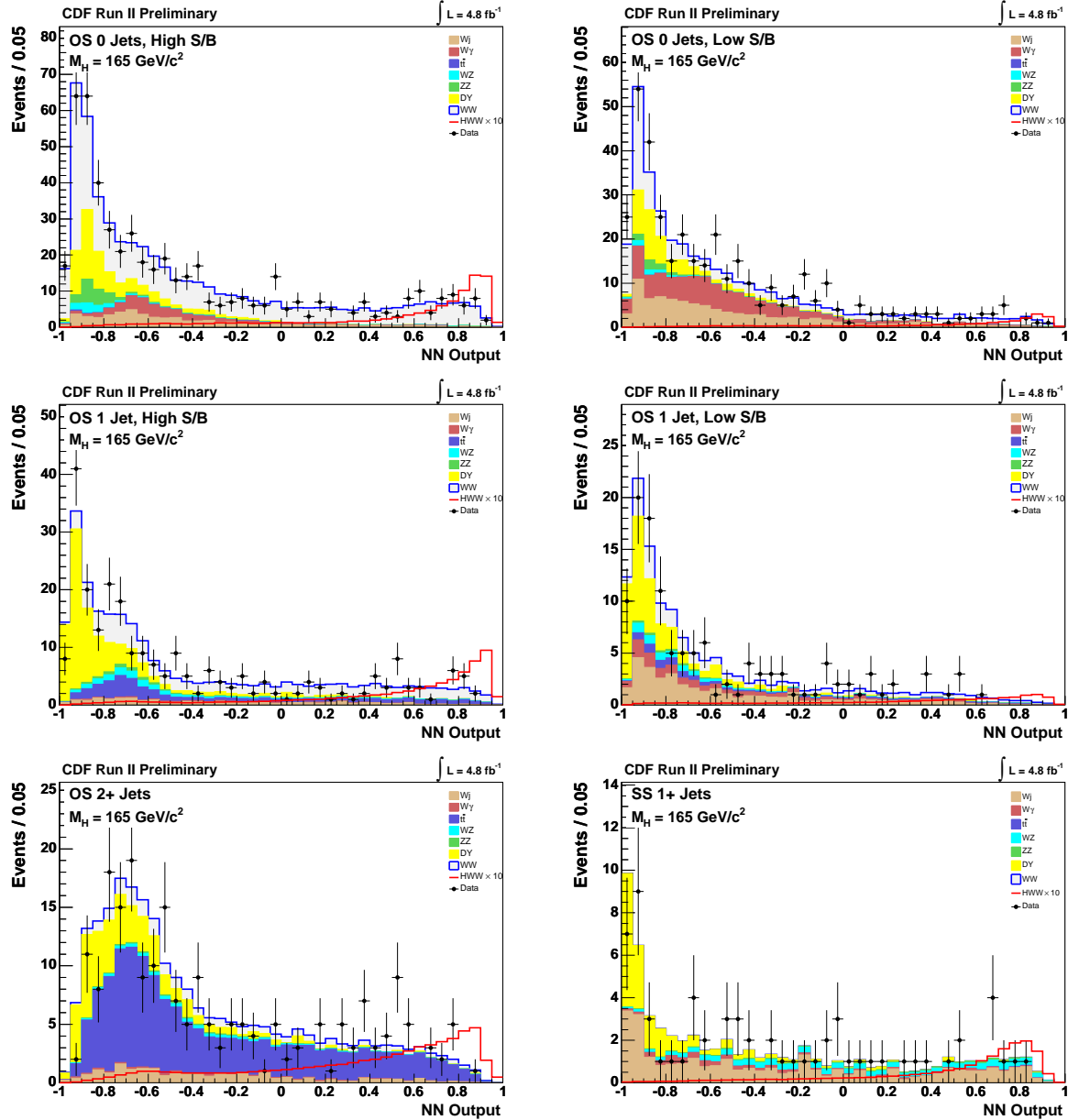


Figure 1: Neural network outputs for each channel (OS zero and one jet for both high and low S/B, OS two or more jets, and SS one or more jets) at $m_H = 165 \text{ GeV}/c^2$. The Higgs boson signal is shown at 10 times the SM prediction.

additional uncertainty of 20% from the detector material description and conversion veto efficiency. The systematic uncertainty on the W +jets background contribution is determined from differences in the measured probability that a jet is identified as a lepton for jets collected using different jet E_T trigger thresholds. These variations correspond to changing the parton composition of the jets and the relative amount of contamination from real leptons.

The cross section calculation uncertainties are 6% on diboson production, 10% on $t\bar{t}$ and $W\gamma$ production, and 5% on Drell-Yan production. All signal and background estimates obtained from simulation have

an additional 6% uncertainty originating from the luminosity measurement [20].

Most systematic uncertainties on the signal processes are assessed using the same techniques described for the background processes. Uncertainties on the theoretical cross sections vary by Higgs boson production mechanism. Associated production cross sections are known to NNLO, so the theoretical uncertainty on these cross sections is small, less than 5% [16]. VBF production is known only to NLO, so the residual theoretical uncertainty is higher, on the order of 10% [16]. Gluon fusion is a QCD process; thus the theoretical uncertainty is still signifi-

cant even though it is known to NNLO. We use the HNNLO program [21, 22], which computes the theoretical cross section for $gg \rightarrow H$ production at the Tevatron to NNLO, to assign theoretical uncertainties due to changing the renormalization and factorization scales (11%) and the gluon PDF model (5%). We again use the HNNLO program to evaluate acceptance uncertainties for $gg \rightarrow H$ production for both changes in scale and the PDF model. To evaluate the change in acceptance, we reweight the Higgs boson p_T and η distributions obtained from PYTHIA to match the HNNLO calculations. Reweighting events based on Higgs boson p_T changes the relative acceptances for the jet channels, while reweighting events based on Higgs boson η primarily affects the lepton acceptance.

7. Results

To determine the sensitivity we construct a binned likelihood using the six neural network templates shown in Figure 1: two templates each for the OS zero and one jet channels (high S/B and low S/B), one template for the OS two or more jets channel, and one template for the SS one or more jets channel. All the signal and background normalizations are allowed to float, but ratios of signal and background contributions are constrained to their expectations with a set of Gaussian constraints determined from the systematic uncertainties. The total signal yield is allowed to float.

The 95% C.L. limits are determined with a set of 50,000 Monte Carlo background-only experiments based on expected yields varied within the assigned systematics. For each experiment a test statistic is formed from the difference in the likelihood value for the background-only model versus that for the signal plus background model. The median expected 95% C.L. limit at a Higgs mass of $165 \text{ GeV}/c^2$ is $1.3^{+0.6}_{-0.4}$ times the SM prediction, while the observed limit is 1.3 times the SM prediction. Results for 14 values of m_H are shown in Table I and Figure 2.

Acknowledgments

We thank the Fermilab staff and the technical staffs of the participating institutions for their vital contributions. This work was supported by the U.S. Department of Energy and National Science Foundation; the Italian Istituto Nazionale di Fisica Nucleare; the Ministry of Education, Culture, Sports, Science and Technology of Japan; the Natural Sciences and Engineering Research Council of Canada; the National Science Council of the Republic of China; the Swiss National Science Foundation; the A.P. Sloan Foundation; the

Bundesministerium für Bildung und Forschung, Germany; the World Class University Program, the National Research Foundation of Korea; the Science and Technology Facilities Council and the Royal Society, UK; the Institut National de Physique Nucleaire et Physique des Particules/CNRS; the Russian Foundation for Basic Research; the Ministerio de Ciencia e Innovación, and Programa Consolider-Ingenio 2010, Spain; the Slovak R&D Agency; and the Academy of Finland.

References

- [1] M. Spira, arXiv:hep-ph/9810289.
- [2] D. de Florian and M. Grazzini, Phys. Lett. B **674**, 291 (2009).
- [3] C. Anastasiou, R. Boughezal, and F. Petriello, J. High Energy Phys. **0904**, 003 (2009).
- [4] A. D. Martin, W. J. Stirling, R. S. Thorne, and G. Watt, Eur. Phys. J. C **63**, 189 (2009).
- [5] A. Abulencia *et al.* (CDF Collaboration), J. Phys. G **34**, 2457 (2007).
- [6] A. Bhatti *et al.*, Nucl. Instrum. Meth. A **566**, 375 (2006).
- [7] R. Brun, R. Hagelberg, M. Hansroul, and J. C. Lassalle, version 3.15, CERN-DD-78-2-REV.
- [8] S. Frixione and B. R. Webber, J. High Energy Phys. **0206**, 029 (2002).
- [9] T. Sjostrand, S. Mrenna, and P. Skands, J. High Energy Phys. **0605**, 026 (2006).
- [10] U. Baur, T. Han, and J. Ohnemus, Phys. Rev. D **57**, 2823 (1998).
- [11] H. L. Lai *et al.* (CTEQ Collaboration), Eur. Phys. J. C **12**, 375 (2000).
- [12] S. Moch and P. Uwer, Nucl. Phys. Proc. Suppl. **183**, 75 (2008).
- [13] J. M. Campbell and R. K. Ellis, Phys. Rev. D **60**, 113006 (1999).
- [14] C. Anastasiou, L. J. Dixon, K. Melnikov, and F. Petriello, Phys. Rev. D **69**, 094008 (2004).
- [15] K. A. Assamagan *et al.* (Higgs Working Group Collaboration), arXiv:hep-ph/0406152.
- [16] TEV4LHC Working Group, <http://maltoni.home.cern.ch/maltoni/TeV4LHC/SM.html>
- [17] M. Feindt and U. Kerzel, Nucl. Instrum. Meth. A **559**, 190 (2006).
- [18] CDF Collaboration, http://www-cdf.fnal.gov/physics/new/hdg/results/hwwmenn_090710/
- [19] S. Kretzer, H. L. Lai, F. I. Olness, and W. K. Tung, Phys. Rev. D **69**, 114005 (2004).
- [20] D. Acosta *et al.*, Nucl. Instrum. Methods Phys. Res., Sect. A **494**, 57 (2002).
- [21] S. Catani and M. Grazzini, Phys. Rev. Lett. **98**, 222002 (2007).

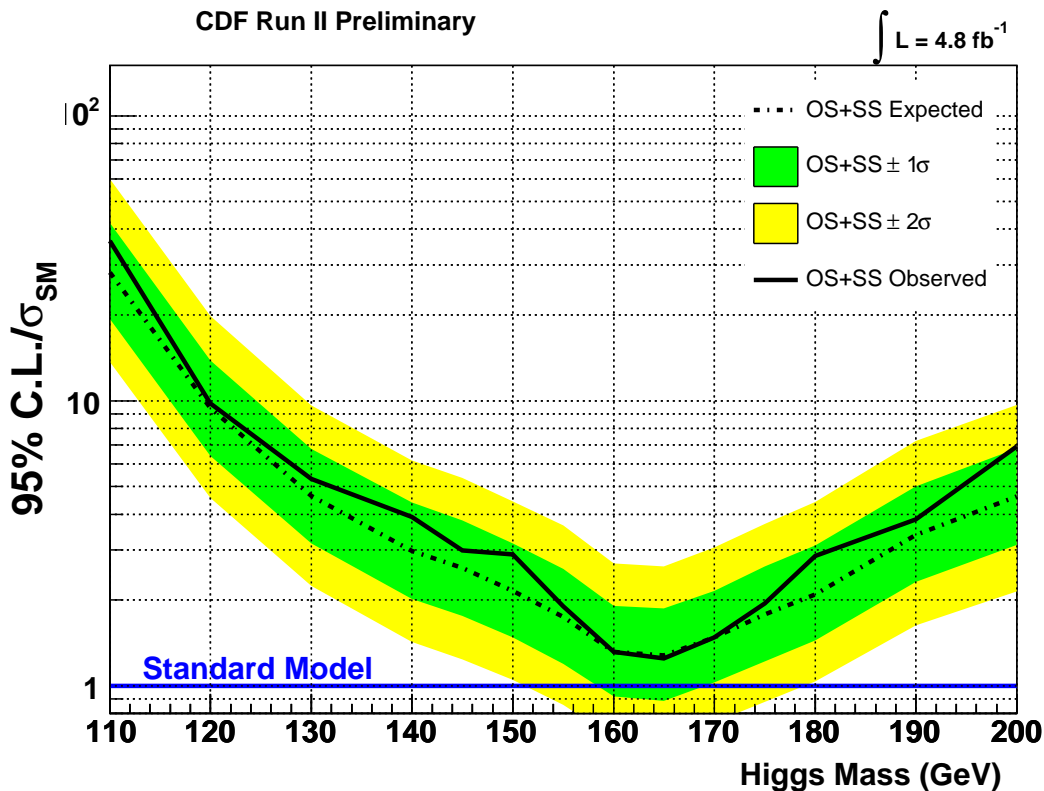


Figure 2: The ratio of expected and observed 95% C.L. production cross section limits to SM predictions for 14 different Higgs boson masses for the combination of all opposite-sign and same-sign $H \rightarrow WW^{(*)}$ decay channels. Error bands are shown on the expected limit, while the observed limit is shown as a solid line.

Table I The ratio of expected and observed 95% C.L. production cross section limits to SM predictions for 14 different Higgs boson masses for the combination of all opposite-sign and same-sign $H \rightarrow WW^{(*)}$ decay channels.

m_H (GeV/ c^2) =	110	120	130	140	145	150	155	160	165	170	175	180	190	200
$-2\sigma/\sigma_{SM}$	13.70	4.55	2.24	1.42	1.24	1.05	0.86	0.66	0.64	0.74	0.88	1.04	1.63	2.14
$-1\sigma/\sigma_{SM}$	19.38	6.41	3.15	2.01	1.76	1.48	1.19	0.92	0.89	1.03	1.22	1.45	2.31	3.12
Median/σ_{SM}	28.23	9.45	4.63	2.97	2.59	2.15	1.74	1.32	1.28	1.48	1.78	2.09	3.39	4.61
$+1\sigma/\sigma_{SM}$	41.99	13.85	6.79	4.39	3.81	3.16	2.57	1.91	1.87	2.16	2.62	3.11	5.01	6.81
$+2\sigma/\sigma_{SM}$	60.07	19.83	9.61	6.18	5.35	4.44	3.65	2.68	2.63	3.06	3.70	4.42	7.23	9.68
Observed/σ_{SM}	36.44	9.78	5.33	3.92	2.99	2.89	1.90	1.31	1.25	1.48	1.95	2.86	3.84	6.93

[22] M. Grazzini, J. High Energy Phys. **0802**, 043 (2008).